A Subspace Identification Technique for Real time Stability Assessment of Droop Based Microgrids

A. F. Elhamalawy, M. E. Ammar, Member, *IEEE*, Hatem F. Sindi, *Member, IEEE*, M. F. Shaaban, *Senior Member, IEEE*, and H. H. Zeineldin, *Senior Member, IEEE*

***Abstract*—Real time detection of the microgrid stability is crucial for determining and adjusting the power-sharing droop controllers' gains to maintain a sufficient stability margin. Maintaining minimum relative stability should be ensured at different operating conditions to accommodate any sudden system changes. This paper develops a novel subspace-based identification technique to assess microgrid stability real time without relying on offline analytical small or large-signal models. Unlike conventional system identification techniques that require the introduction of external excitation signals, the proposed method employs a simple routine through small and short-duration perturbations in the active power droop gain of inverter-based distributed generation (IBDG). The use of subspace identification does not require pre-defining the system's order and avoids the exhaustive computations associated with iterative identification methods. The proposed stability assessment method has been tested on an IBDG microgrid considering different operating conditions in MATLAB/Simulink. The accuracy of the proposed real time stability assessment tool is determined by comparing the results to the analytically-derived small-signal model.**

***Index Terms*—Droop control, Microgrid, Stability assessment, Subspace identification, Distributed generation**

I. Introduction

In recent years, penetration of renewable energy sources (RES) in traditional electrical networks surged significantly to reduce fossil fuel consumption and consequently minimize carbon dioxide emissions. This led to an increase in the RES installed capacity and motivated the formation of microgrids that can be operated in both grid-connected and islanded modes. Due to the low inertia of microgrids in the islanded mode, control and power management require thorough analysis to ensure voltage and frequency quality in addition to system stability [1]. Multiple techniques have been developed to control the challenging operation of the low inertia microgrids in the islanded mode [2]. An extensive review of active and reactive power sharing methods was presented in [3]. The droop controller originally proposed in [4] emulates the behavior of traditional synchronous generators providing a low-cost communication-free power-sharing solution. The conventional droop controller shares active and reactive power through regulating the microgrid's frequency and individual inverter's output voltage, respectively [5]. The droop controller provides reference settings for the voltage and current control loops in the primary control level that is based on local measurements. A supplementary secondary control layer is required to restore frequency and voltage deviations caused by primary droop controllers [6], [7], [8], and [9]. In [10], the secondary control level is used to improve the efficiency in a droop-based control scheme. A two-level hierarchical control, including a centralized controller, is proposed to improve the dynamic performance and stability of the microgrid in [7]. A tertiary control level is adopted in a hierarchical microgrid control structure to ensure optimal power flow and economic operation [11], [12], and [13]. A review of the control levels and a comparison between the various control structures are given in [14]. Hierarchical, distributed, and decentralized control approaches are reviewed and discussed in [15] and [16].

Investigating small signal stability is an important issue for inverter-based distributed generation (IBDG) microgrids [5], [17], [18], [19] and [20]. The power-sharing droop controller, along with the low pass filter loops, introduces low-frequency modes that can reduce the relative stability of the microgrid [17] and [21]. The droop gains must be chosen properly to ensure a satisfactory transient response without compromising the dynamic stability of the microgrid. It has been shown that an IBDG microgrid's domain of stability changes in the case of line or DG disconnections in [22]. Analytical conditions for the small-signal stability of practical microgrids based on droop gains and network parameters are given in [23].

In [24], an adaptive control approach is proposed to improve the dynamic stability and performance of microgrids through the scheduling of transient droop gains. An adaptive feedforward compensator was developed to enhance the system stability of droop-based microgrids in [25]. The voltage droop was adaptively tuned to facilitate accurate reactive power sharing in [26]. Adaptive droop gains combined with varying virtual impedances are proposed to handle power fluctuations in microgrids with renewable energy sources in [27]. The authors in [28] proposed an accurate power-sharing via adaptive virtual impedance within a hierarchical control structure. An adaptive power droop is proposed to improve the dynamic stability and response when the microgrid is subject to

Abdallah F. Elhamalawy, Mohammed E. Ammar and H. H. Zeineldin are with the Electrical Power Engineering Dep., Cairo University, Giza 12613, Egypt H. H. Zeineldin is currently on leave from Khalifa University. Corresponding Author: M.E. Ammar (e-mail:mohammed.ammar@cu.edu.eg).

Hatem F. Sindi is with the department of Electrical and Computer Engineering in King Abdulaziz University, Jeddah, Saudi Arabia (hfsindi@kau.edu.sa). M. F. Shaaban is with the American University of Sharjah, Sharjah, UAE.

 DOI:"10.1109/TPWRS.2021.3126809"

disturbances in [29].

A successful adaptive control scheme must be combined with an online tool to assess microgrid dynamic stability at different droop gains and loading conditions. As the microgrid increases in size with respect to the number of DGs, lines, and nodes, small signal stability analysis becomes a computational burden due to the large dimension of the state-space models. One solution to deal with this challenging problem is to rely on reduced-order models. In [30], three different reduced-order network modeling techniques are discussed and compared to determine their accuracies regarding eigenvalues, stability bounds, and damping ratio. Although the model reduction approach is computationally efficient, it relies on an offline analytical derivation modeling based on a static deterministic network.

In this paper, a novel real time stability assessment approach that adopts system identification is developed for inverter-based microgrids. The proposed technique will enable monitoring microgrid dynamic stability online based on real measurements and thus allowing for corrective actions to be taken to increase relative stability or stability margins. This assessment tool is to be incorporated in a hierarchical control scheme which would allow the secondary control level to tune the droop controllers adaptively while assessing stability online without resorting to complex offline analysis. The developed method adopts subspace identification techniques to determine the dominant eigenvalues and, consequently, relative stability, stability margin, and damping ratio of the oscillatory modes. The proposed technique relies on introducing a small pulsed perturbation in a DG's active power droop gain followed by collecting real-time measurements to estimate a reduced-order model that is used to assess the current stability state of the islanded microgrid accurately.

The rest of the paper is organized as follows; Section II briefly reviews the small-signal model of an IBDG microgrid. The use of the subspace identification technique to assess the microgrid's stability is presented in Section III. In Section IV, the simulation results for various case studies are presented and discussed. Finally, conclusions are summarized in Section V.

II. Small-Signal Model

The small-signal model for a droop-controlled islanded microgrid at a specific operating point is derived in [17]. One of the main advantages of the given procedure is its flexibility to accommodate any number of DGs and nodes. A typical IBDG control system interface is illustrated in Fig. 1. The output voltage and current are transformed to dq- components in a rotating frame at an angular frequency (ω). The instantaneous active and reactive power values are computed from the voltage, and current expressed in the dq-frame then are filtered through a low pass filter. The average values of the active and reactive powers are fed to the power controller to set the frequency and the reference voltage. The voltage controller sets the reference current to the current controller, which is the innermost loop in this control scheme. Standard proportional-integral (PI) controllers are implemented in the voltage and current control loops. The small-signal model of each DG is a combination of a set of small-signal models of droop controller, voltage controller, current controller, the output filter, and coupling inductance.

The model of the i^{th} DG can be expressed as:

$$[\Delta x_{INVi}] = A_{invi}[\Delta x_{INVi}] + B_{INVi}[\Delta V_{bDQi}] + B_{i\omega com}[\Delta\omega_{com}], \quad (1)$$

$$\begin{bmatrix}\Delta\omega_i \\ \Delta i_{oDQi}\end{bmatrix} = \begin{bmatrix}C_{INV\omega i} \\ C_{INVci}\end{bmatrix}[\Delta x_{INVi}] \quad (2)$$

$[\Delta x_{INVi}] = [\Delta\delta_i \ \Delta P_i \ \Delta Q_i \ \Delta\phi_{dqi} \ \Delta\gamma_{dqi} \ \Delta i_{ldqi} \ \Delta v_{odqi} \ \Delta i_{odqi}]^T$,

where Δ represents the small signal variation, δ_i corresponds to the angle between each inverter's local reference frame and the global frame, (P_i, Q_i) are the active and reactive powers, $(\phi_{dqi}, \gamma_{dqi})$ are the integration of the errors in the DQ voltage and current components, respectively while the remaining states $(i_{ldqi}, i_{odqi}, v_{odqi})$ are the dq components of output currents and voltage. $\Delta\omega_{com}$ is the frequency variation of the common rotating reference frame. In order to obtain the complete system model, sub-models for both network and loads were derived and integrated with inverters' models to obtain the overall small-signal model for n_{inv} DGs connected to one network that has n_{node} nodes through n_{line} lines and supplying n_{load} loads. The microgrid small-signal model is given by:

$$\begin{bmatrix}\dot{\Delta X_{INV}} \\ \Delta\imath_{line\ dq} \\ \Delta\imath_{load\ dq}\end{bmatrix} = A_{mg}\begin{bmatrix}\Delta X_{INV} \\ \Delta i_{line\ dq} \\ \Delta i_{load\ dq}\end{bmatrix} \quad (3)$$

where, $\Delta X_{INV}, \Delta i_{line\ dq}, \Delta i_{load\ dq}$ are the combined state vectors of all the individual inverters, network lines, and loads, respectively, as follows:

$$\Delta X_{INV} = [\Delta x_{INV\,1} \quad \Delta x_{INV\,2} \quad \dots \quad \Delta x_{INV\,n_{inv}}]^T$$
$$\Delta i_{line\ dq} = [\Delta i_{line\ dq\,1} \quad \Delta i_{line\ dq\,2} \quad \dots \quad \Delta i_{line\ dq\,n_{line}}]^T$$
$$\Delta i_{load\ dq} = [\Delta i_{load\ dq\,1} \quad \Delta i_{load\ dq\,2} \quad \dots \quad \Delta i_{load\ dq\,n_{load}}]^T$$

The details of all the matrices are given [17] and are omitted here for brevity. Investigating the system's state matrix A_{mg}, the stability of the overall microgrid is checked based on the location of its eigenvalues along with the damping ratio of the system. The proposed work aims to provide an online tool for assessing the microgrid stability through determining the dominant eigenvalues (modes) of matrix A_{mg} using online measurements only. This is achieved via the subspace identification technique that is discussed in the next section.

III. Stability Assessment Method

A. Subspace Identification

The use of subspace identification (SID) techniques in identifying MIMO systems avoids ill-conditioned mathematical problems, and the requirement of prior parameterization as the system's order can be detected using singular value decomposition of the calculated matrices. An additional advantage in SID is its ability to use a non-iterative method that avoids non-linear optimization problems, as discussed in [31].

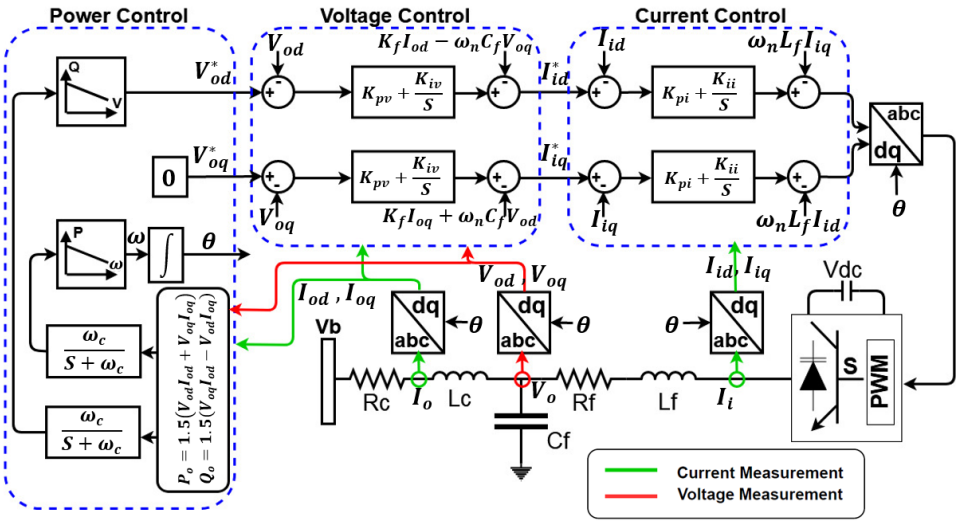

Fig 1. DG droop based interface control

Consider the following Linear Time-Invariant (LTI) discrete deterministic system with l inputs and m outputs,

$$x_{k+1} = Ax_k + Bu_k \quad (4)$$

$$y_k = Cx_k + Du_k \quad (5)$$

where A, B, C, D are states, input, output, and direct matrices respectively, while x_k, u_k, y_k are system's state, input, and output vectors respectively at time instant k.

Using recursive substitution of equations (4) and (5), we can conclude the following matrix input-output equations [31].

$$Y_p = \Gamma_i X_p + H_i U_p \quad (6)$$

$$Y_f = \Gamma_i X_f + H_i U_f \quad (7)$$

$$X_f = A^i X_p + \Delta_i U_p \quad (8)$$

Where,

$$\Gamma_i = [C^T \quad (CA)^T \quad (CA^2)^T \quad \cdots \quad (CA^{i-1})^T]^T$$

$$\Delta_i = [A^{i-1}B \quad A^{i-2}B \quad \ldots \quad AB \quad B]$$

$$H_i = \begin{bmatrix} D & 0 & 0 & \cdots & 0 \\ CB & D & 0 & \cdots & 0 \\ CAB & CB & D & \cdots & 0 \\ \vdots & \vdots & \vdots & \vdots & \vdots \\ CA^{i-2}B & CA^{i-3}B & CA^{i-4}B & \ldots & D \end{bmatrix}$$

$$U_{0|2i-1} = \begin{bmatrix} u_0 & u_1 & & u_{j-1} \\ u_1 & u_2 & & u_j \\ \cdots & \cdots & & \cdots \\ u_{i-1} & u_i & \cdots & u_{i+j-2} \\ u_i & u_{i+1} & & u_{i+j-1} \\ u_{i+1} & u_{i+2} & & u_{i+j} \\ \cdots & \cdots & & \cdots \\ u_{2i-1} & u_{2i} & & u_{2i+j-2} \end{bmatrix}$$

$$= \begin{bmatrix} U_{0|i-1} \\ U_{i|2i-1} \end{bmatrix} = \begin{bmatrix} U_p \\ U_f \end{bmatrix}$$

$$X_p = X_0 = [x_0 \quad x_1 \quad \cdots \quad x_{j-2} \quad x_{j-1}]$$

$$X_f = X_i = [x_i \quad x_{i+1} \quad \cdots \quad x_{i+j-2} \quad x_{i+j-1}]$$

The matrices $\Gamma_i, \Delta_i, and\ H_i$ are known as extended observability, reversed extended controllability, and lower triangular Toeplitz matrices, respectively. U_p, U_f, Y_p and Y_f are the past and future input and output block Hankel matrices, respectively. Each Hankel matrix consists of i rows and j columns. The subscript $\bullet_p$ stands for the past while $\bullet_f$ stands for future data. It is important to state that the selection of number of rows i should be larger than expected system's order while j expresses the length of identification data.

From equations (7) and (8), the future block Hankel output matrix can be rewritten as follows:

$$Y_f = \left[\Gamma_i(\Delta_i - A^i\Gamma_i^+ H_i) \quad \Gamma_i A^i \Gamma_i^\dagger\right] W_p + H_i U_f \quad (9)$$

Where, $W_p = \begin{bmatrix} U_p \\ Y_p \end{bmatrix}$

- $\bullet^\dagger$ denotes the Moore-Penrose pseudo-inverse

Hence, by means of oblique projection, the past input and output component of Y_f can be extracted as:

$$O_i = Y_f /_{U_f} W_p = \Gamma_i X_f \quad (10)$$

The extended observability matrix Γ_i is easily decomposed using singular value decomposition:

$$O_i = [U_1 \quad U_2] \begin{bmatrix} S_1 & 0 \\ 0 & 0 \end{bmatrix} \begin{bmatrix} V_1^T \\ V_2^T \end{bmatrix} = U_1 S_1 V_1^T \quad (11)$$

$$\Gamma_i = W_1^{-1} U_1 S_1^{1/2} \quad (12)$$

System matrices (A and C) can be calculated as follows:

$$C = first\ l\ rows\ of\ \Gamma_i$$

$$A = \underline{\Gamma_i}^+ \overline{\Gamma_i}$$

Where $\overline{\Gamma_i}$ denotes the matrix Γ_i without the first l rows

$$\underline{\Gamma_i} A = \overline{\Gamma_i}$$

Conversely, extraction of B and D matrices starts by multiplying equation (7) by $\Gamma_i^\perp$ from the left which results in:

$$\Gamma_i^\perp Y_f U_f^\dagger = \Gamma_i^\perp H_i \quad (13)$$

For simplicity, denote the left-hand side by M and $\Gamma_i^\perp$ by L.

$$M = LH_i \quad (14)$$

Then extraction of B and D matrices is obtained by rewriting the previous equation and solving the least square problem:

$$\begin{bmatrix} M_1 \\ M_2 \\ \vdots \\ M_i \end{bmatrix} = \begin{bmatrix} L_1 & L_2 & \ldots & L_i \\ L_2 & L_3 & \ldots & 0 \\ \cdots & \cdots & \cdots & 0 \\ L_i & 0 & \ldots & 0 \end{bmatrix} \begin{bmatrix} I_l & 0 \\ 0 & \underline{\Gamma_i} \end{bmatrix} \begin{bmatrix} D \\ B \end{bmatrix} \quad (15)$$

Fig. 2 illustrates the steps required for the subspace identification technique.

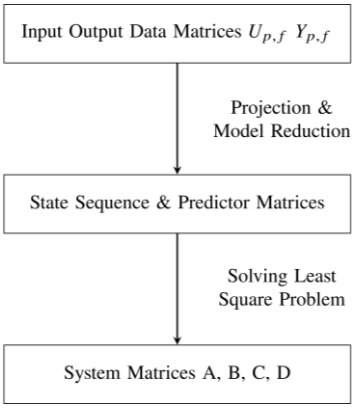

Fig. 2. Flowchart of the subspace identification approach.

B. *Online Stability Assessment Algorithm*

As discussed in section II, the microgrid small-signal model at a specific operating point is represented by an autonomous state matrix A_{mg}. The stability assessment algorithm adopts the subspace identification tools to determine the dominant modes of an autonomous microgrid when operating at a certain loading condition. In other words, the algorithm will periodically estimate the matrix $\hat{A}_{mg}$ and its eigenvalues by means of real-time measurements. Fig. 3 illustrates the complete block diagram of the proposed algorithm, where the droop gain of one of the DGs is disturbed by the exciter, and real-time measurements (angle, active power, reactive power, line, and load currents) are collected, filtered, and fed to the subspace analyzer. The amount of active droop gain excitation Δm_p is chosen as a compromise between limiting the perturbation to be as small as possible to the operating point and producing sufficient excitation to ensure correct estimation of the dominant eigenvalues. Typically, this disturbance is to be limited to 2%. The construction of subspace analyzer is very similar to the conventional subspace identification. However, as the microgrid model is represented by an autonomous state space as given in equation (16); the construction will be tailored for autonomous models.

$$\begin{aligned} \dot{X_{mg}} &= A_{mg}X_{mg} \\ Y_{mg} &= C_{mg}X_{mg} \end{aligned} \tag{16}$$

where, C_{mg} is an identity matrix. The oblique projection O_i given by equation (11) will be modified, and then singular value decomposition (svd) is performed to determine the system's order.

$$O_i = Y_{mg} = \Gamma_i \hat{X}_{mg} \tag{17}$$

After that, the microgrid's state and output matrices $\hat{A}_{mg}$, $\hat{C}_{mg}$ are estimated using the extended observability matrix Γ_{i}.

$$\begin{aligned} \hat{A}_{mg} &= \underline{\Gamma_i^{+}}\overline{\Gamma_{\mathrm{i}}} \\ \hat{C}_{mg} &= first\ l\ rows\ of\ \Gamma_{\mathrm{i}} \end{aligned} \tag{18}$$

The identified state sequence $\hat{X}_{mg}$ is not necessarily in the same order as the state vector derived in equation (3). A full order estimated state-space model representation is related to the original small signal model by:

$$\begin{aligned} \hat{A}_{mg} &= \mathrm{T}^{-1}A_{mg}T \\ \hat{C}_{mg} &= C_{mg}T \end{aligned} \tag{19}$$

where, T is a transformation matrix. Nevertheless, given the non-uniqueness of state-space models the eigenvalues of both representations are the same as given in (20).

$$eigen\ values\ (\hat{A}_{mg}) = eigen\ values\ (A_{mg}) \tag{20}$$

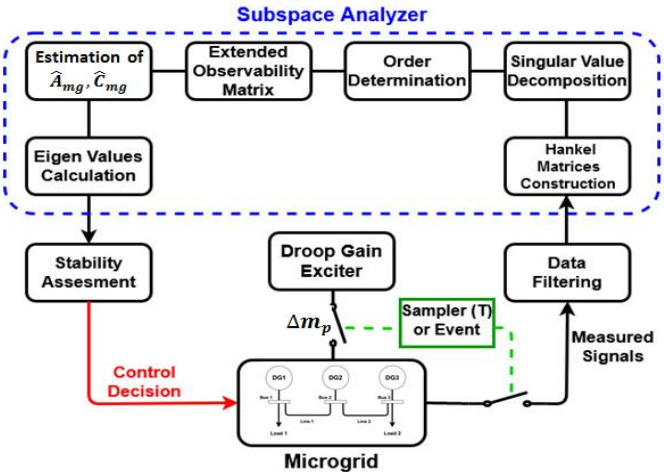

Fig. 3. Stability Assessment Algorithm Block Diagram

Stability assessment is based on evaluating the location of the eigenvalues after remapping the discrete eigenvalues to the continuous domain by the transformation $s = \frac{\ln(z)}{T_s}$ where T_s is the sampling time used in the identification. Based on stability assessment, a control decision should be taken to enhance the microgrid's stability. The whole cycle is repeated periodically every time T which is selected based on the computation capabilities of the available controller. In addition, stability assessment could be initiated by some pre-defined events such as disconnection of a DG or network reconfiguration.

IV. Case Studies

The IBDG microgrid setup given in [17] is considered for validating the developed online stability assessment tool. The network has three identical DGs (10 KVA rating) that are connected by means of two lines to supply two loads connected to bus1 and bus3, as illustrated by Fig. 4. The nominal phase voltage is 220 V, and the frequency is 50 Hz. The main parameters of this microgrid are given in Table I. $\mathrm{m_{p0}}$ is the nominal active power droop gain.

The viability of the developed technique was tested via three different case studies. The effect of active power droop changes is considered in the first case study, while the second one considers the effect of changing the microgrid X/R ratio, which imitates a partial change in network parameters. In these cases, the droop gain perturbation is introduced at DG1. The last case study considers the influence of changing the excitation location on the accuracy of estimating the system's dominant modes where DG2 is chosen as the alternative location. The

perturbation in the droop gain m_p is a positive pulse with a width of 0.5 second and amplitude of $0.02m_p$

TABLE I
MICROGRID PARAMETERS

Parameter	Value	Parameter	Value
R_f	0.1	R_{line2}	0.35
L_f	1.35e-3	L_{ine2}	1.85e-3
C_f	50e-6	R_{load1}	25
R_C	0.03	L_{load1}	0.1e-1
L_C	0.35e-3	R_{load2}	25
R_{line1}	0.23	L_{load2}	0.1e-1
L_{line1}	0.35e-3	m_{po}	9.5e-5

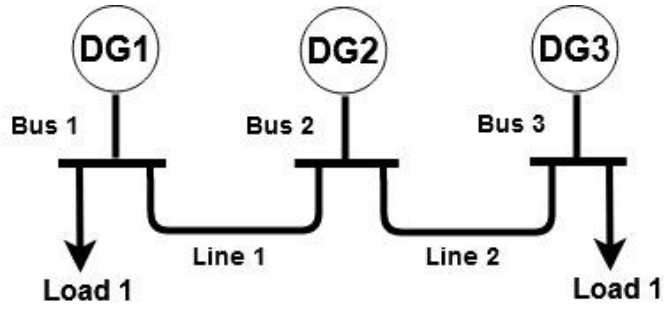

Fig. 4. Single Line Diagram of the Microgrid

A. *Effect of Changing Droop Gain*

The effect of changing the active power droop gain m_p on the accuracy of the subspace analyzer, in estimating the primary and secondary dominant modes, was investigated for three different values of m_p. Estimated modes are plotted against the actual modes, obtained from the small-signal model which was derived analytically, in Fig. 5. It is clear that the dominant modes move towards the $J\omega$-axis as m_p increases, and that the estimated modes are very close to the exact values determined by the offline small-signal model for all three droop values.

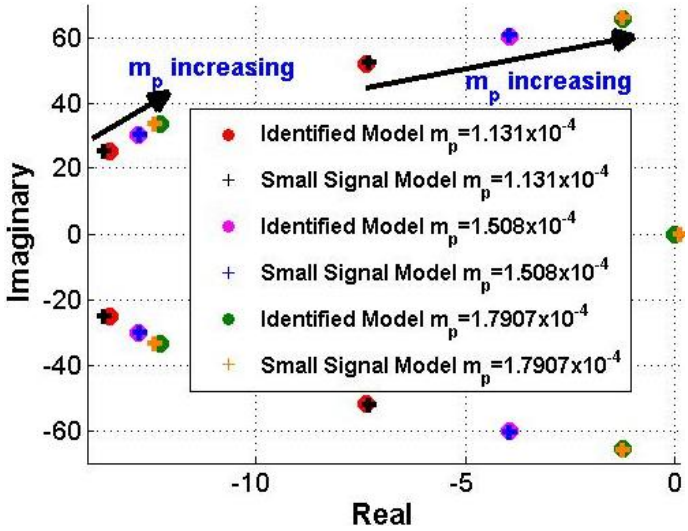

Fig. 5. Actual and Estimated Dominant Modes at Different Droop Gains

The active power-sharing among the DGs is mainly dependent on the value of its droop gain m_p, hence disturbing one of the DGs active power droop will redistribute the power-sharing slightly among the different DGs during the perturbation period. Since the droop gain m_p excitation is a temporary pulse; the power-sharing will be restored to the equal power-sharing state. Fig. 6, Fig. 7, and Fig. 8 present the DGs active and reactive power as well as their phase angles subsequent to the excitation period. As can be seen, the estimated waveforms using the proposed approach closely match the microgrid simulation results. Furthermore, prior and subsequent to the excitation period, the three DGs share the active power equally. During the excitation period, DG1 which is the DG at which the perturbation occurs, provides less active power than the two other DGs.

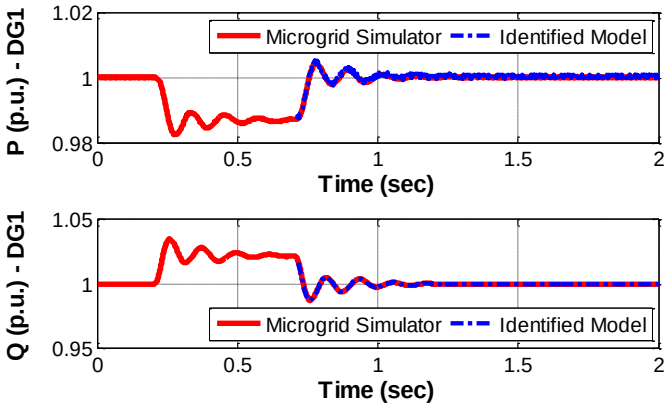

Fig. 6. Identified active and reactive power signals of DG1 vs. the real measurements of microgrid simulator at droop gain $m_p = 1.131 * 10^{-4}$

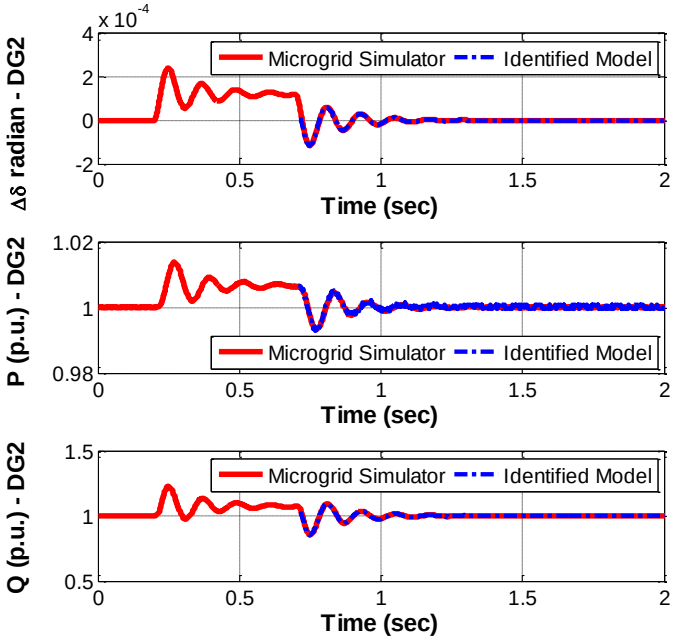

Fig. 7. Identified angle, active and reactive power signals of DG2 vs. real measurements of microgrid simulator at droop gain $m_p = 1.131 * 10^{-4}$

Table II summarizes the results obtained for the three cases and indicates the percentage error in the estimation of each mode. The obtained results highlight the precision and accuracy of the proposed online stability assessment tool for inverter-

based microgrids. The percentage error for all modes is within 2 percent.

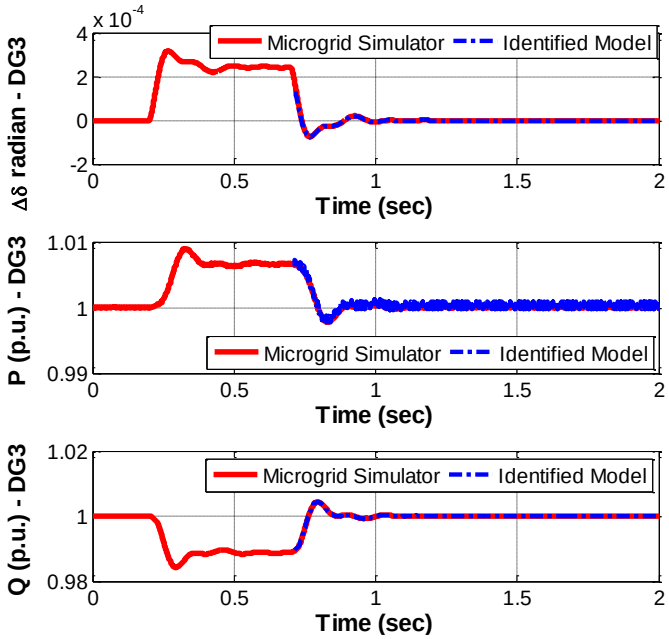

Fig. 8. Identified angle, active and reactive power signals of DG3 vs. real measurements of microgrid simulator at droop gain $m_p = 1.131 * 10^{-4}$

TABLE II
ACCURACY OF ESTIMATING PRIMARY AND SECONDARY DOMINANT MODES AT DIFFERENT DROOP GAINS

$m_p x 10^{-4}$	Actual Modes	Estimated Modes	% Error in Real Part	% Error in Imaginary Part
1.131	$-7.34086 \pm 51.7304J$	$-7.28892 \pm 52.0933J$	0.70754	0.7016
	$-13.4517 \pm 25.1579J$	$-13.5875 \pm 25.0455J$	1.0098	0.44696
1.508	$-3.95562 \pm 60.272J$	$-3.93567 \pm 60.4689J$	0.50419	0.32679
	-12.7773 ± 30.3857	$-12.7538 \pm 30.3232J$	0.18348	0.20571
1.7907	$-1.23676 \pm 65.5698J$	$-1.26065 \pm 65.8443J$	1.9315	0.41871
	$-12.2472 \pm 33.7134J$	$-12.3913 \pm 33.5906J$	1.1762	0.36437

B. *Effect of X/R Ratio*

In order to further validate the proposed online identification technique, the X/R ratio of the lines have been varied, and the system was tested for different values of m_p. Four tests have been established to investigate the accuracy at different X/R ratios. The X/R ratio of the first transmission line is doubled, and the estimation process is performed twice at $m_p = 1.6965x10^{-4}$ *and* $m_p = 2.262x10^{-4}$. Similar tests were performed while halving the X/R ratio of the second transmission line at different droop gains $m_p = 9.424x10^{-4}$ *and* $m_p = 1.3195x10^{-4}$. Fig. 9 presents the actual dominant modes for all cases versus the estimated ones. As $m_p$increases the modes move towards the $J\omega$-axis. More importantly, the results in Fig. 9 highlight the close match between the identified dominant modes determined using the proposed approach and the derived small-signal model considering the various X/R ratio. Real measurements collected for identifying the dominant modes are compared to the estimated data obtained by means of the subspace technique to show the accuracy of the estimation model. Fig. 10 to Fig. 12 show a sample of the measurements and the estimated signals of DG1, DG2, and DG3, respectively, when the X/R ratio of the second line is halved while setting $m_p = 1.3195 * 10^{-4}$. Similarly, subsequent to the excitation period, all DGs share the active power equally, and more importantly, the signals obtained using the identified model closely match the micro-grid simulation results.

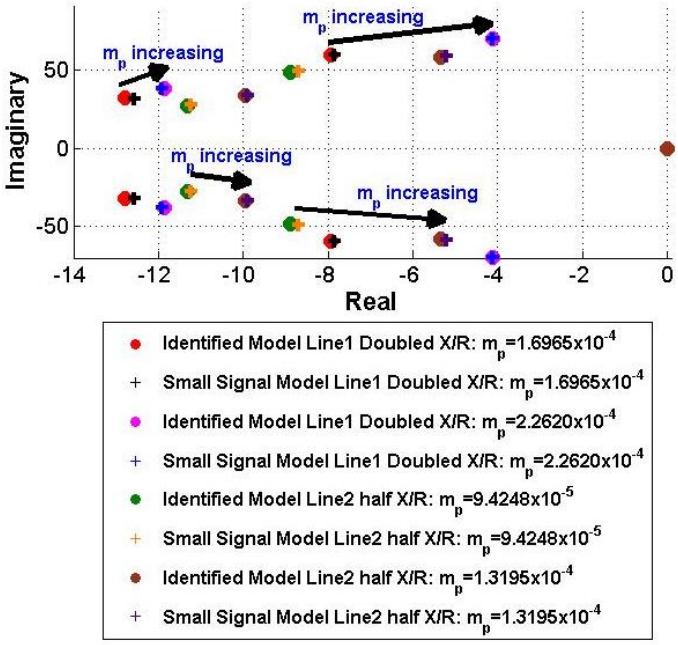

Fig. 9. Actual and Estimated Dominant Modes for different X/R Ratios and Different Droop Gains

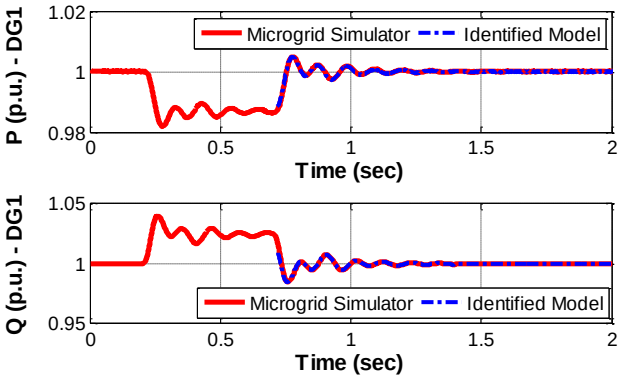

Fig. 10. Identified active and reactive power signals of DG1 vs. real measurements of microgrid simulator at droop gain $m_p = 1.3195 * 10^{-4}$ while line2 X/R ratio is halved

Further details on the accuracy of the system identification and the percentage error in the estimated modes are given in Table III and Table IV. The maximum percentage error for the case where the X/R ratio is doubled is less than 2 percent, while for the case where the X/R ratio was halved, the percentage error is within 3 percent. As can be seen, the system X/R ratio has a tolerable effect on the accuracy of the proposed identification technique.

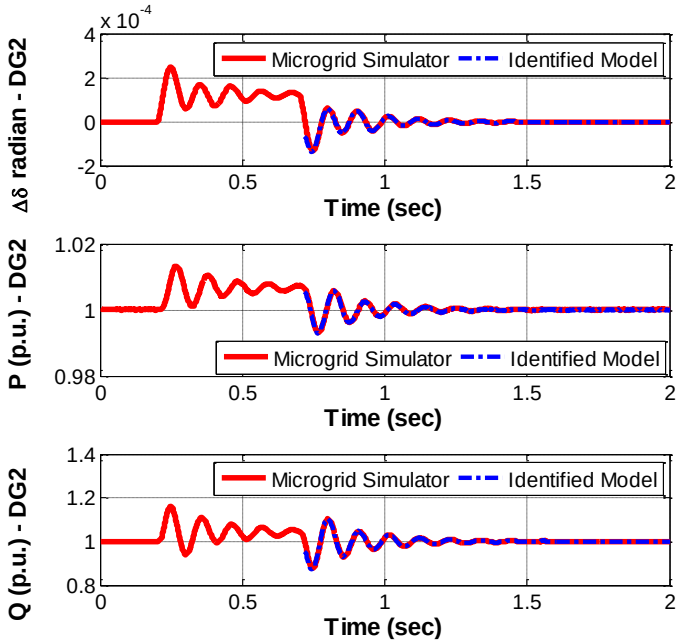

Fig. 11. Identified angle, active and reactive power signals of DG2 vs. real measurements of microgrid simulator at droop gain $m_p = 1.3195 * 10^{-4}$ while line2 X/R ratio is halved

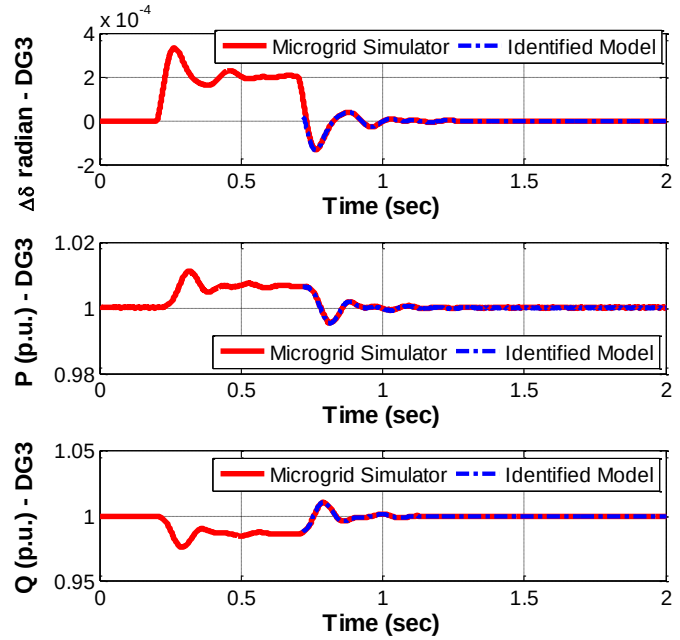

Fig. 12. Identified angle, active and reactive power signals of DG3 vs. real measurements of microgrid simulator at droop gain $m_p = 1.3195 * 10^{-4}$ while line2 X/R ratio is halved

TABLE III
ACCURACY OF ESTIMATING PRIMARY AND SECONDARY DOMINANT MODES AT DIFFERENT DROOP GAINS WHEN LINE1 X/R RATIO IS DOUBLED

$m_p x 10^{-4}$	Actual Modes	Estimated Modes	% Error in Real Part	% Error in Imaginary Part
1.6965	$-7.93002 \pm 59.2415J$	$-7.84852 \pm 59.6612J$	1.0277	0.70847
	$-12.7809 \pm 31.7661J$	$-12.5674 \pm 31.7063J$	1.6703	0.18817
2.262	$-4.11861 \pm 69.4012J$	$-4.12447 \pm 69.5439J$	0.4189	0.51226
	$-11.8716 \pm 37.6962J$	$-11.9213 \pm 37.8893J$	0.14235	0.20562

TABLE IV
ACCURACY OF ESTIMATING PRIMARY AND SECONDARY DOMINANT MODES AT DIFFERENT DROOP GAINS WHEN LINE2 X/R RATIO IS HALVED

$m_p x 10^{-4}$	Actual Modes	Estimated Modes	% Error in Real Part	% Error in Imaginary Part
0.94248	$-8.89886 \pm 48.3917J$	$-8.70374 \pm 48.8968J$	2.1927	1.0438
	$-11.3199 \pm 27.2715J$	$-11.2227 \pm 27.385J$	0.85875	0.41608
1.3195	$-5.35065 \pm 58.198J$	$-5.20138 \pm 58.6666J$	2.7899	0.80514
	$-9.96273 \pm 33.2294J$	$-9.88941 \pm 33.2445J$	0.73591	0.04546

C. *Effect of Excitation Location*

To further validate the capabilities of the proposed technique and its effectiveness, the stability assessment was conducted while changing the location of excitation. In this test, the excitation was executed within the interface control of DG2. In order to investigate a wider range of operation, the test is performed at different droop gains as in the case studies presented in subsections IV A &B. Table V shows a comparison between the results obtained from the first case study where the perturbation was introduced at DG1 and the new results obtained when the perturbation occurred at DG2. As can be seen from Table V, some differences can be noticed in error estimation from the first case study, but all errors are still within 3 percent.

In Fig. 13, real active and reactive power measurements are plotted versus the estimated data for the second test when $m_p = 1.508 * 10^{-4}$ while exciting DG2 droop. Fig 14 and 15 illustrate the changes in angles, active and reactive power of DG2 and DG3, respectively. During the perturbation period, DG2 supplies less active power than DG1 and DG3 as a result of the perturbation in droop gain. Restoring the droop gain at DG2 to its previous value is followed by an increase in the active power share of DG2 and a gradual equivalent decline in the shares of DG1 and DG3 such that all DGs share the load equally. Similarly, for all DGs, there is a close match between the time domain simulation results and the results obtained using the proposed identification technique.

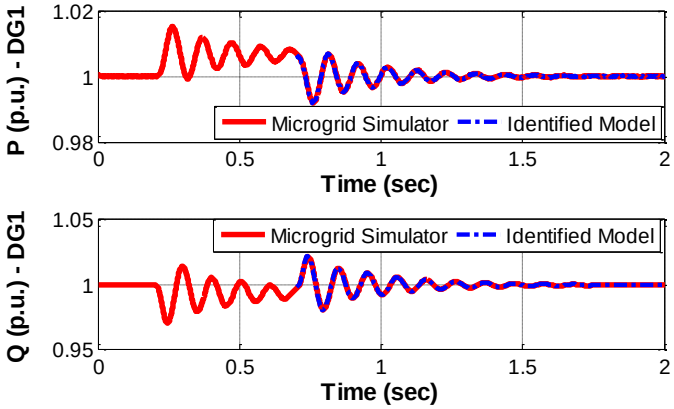

Fig. 13. Identified active and reactive power signals of DG1 vs. real measurements of microgrid simulator at droop gain $m_p = 1.508 * 10^{-4}$ while excitation is located at DG2

TABLE V
COMPARISON OF ESTIMATING PRIMARY AND SECONDARY DOMINANT MODES BASED ON DIFFERENT EXCITATION LOCATIONS

$m_p x 10^{-4}$	Actual Modes	DG1 Excitation			DG2 Excitation		
		Estimated Modes	% Error in Real Part	% Error in Imaginary Part	Estimated Modes	% Error in Real Part	% Error in Imaginary Part
1.131	$-7.34086 \pm 51.7304J$	$-7.28892 \pm 52.0933J$	0.70754	0.7016	$-7.24266 \pm 52.0528J$	1.3377	0.62338
	$-13.4517 \pm 25.1579J$	$-13.5875 \pm 25.0455J$	1.0098	0.44696	$-13.4306 \pm 25.3854J$	0.15664	0.90409
1.508	$-3.95562 \pm 60.272J$	$-3.93567 \pm 60.4689J$	0.50419	0.32679	$-3.8538 \pm 60.3681J$	2.574	0.15947
	-12.7773 ± 30.3857	$-12.7538 \pm 30.3232J$	0.18348	0.20571	$-12.6851 \pm 29.733J$	0.72122	2.1481

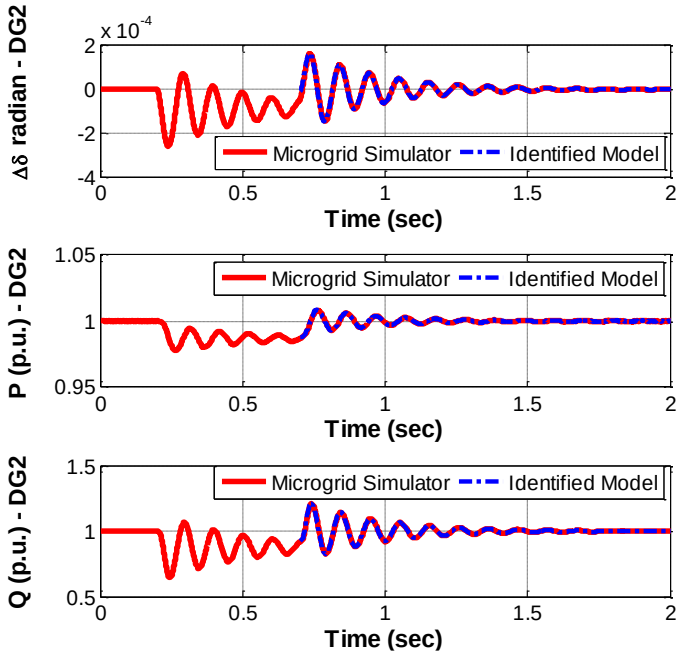

Fig. 14. Identified angle, active and reactive power signals of DG2 vs. real measurements of microgrid simulator at droop gain $m_p = 1.508 * 10^{-4}$ while excitation is located at DG2

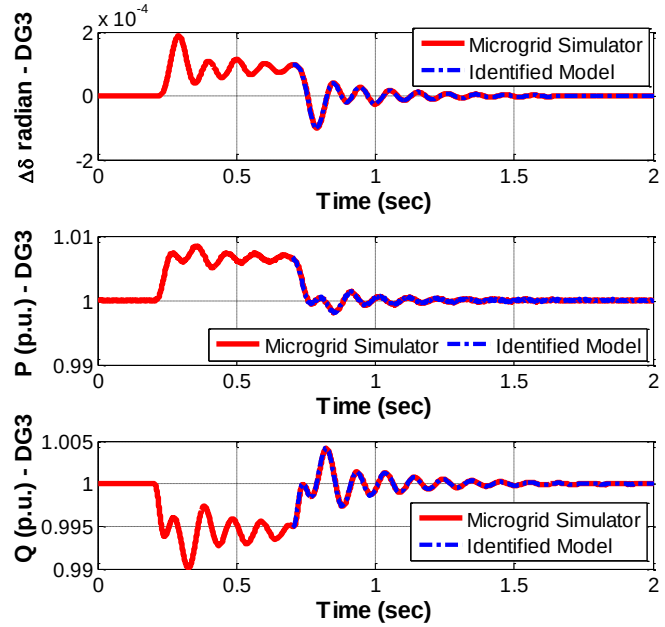

Fig. 15. Identified angle, active and reactive power signals of DG3 vs. real measurements of microgrid simulator at droop gain $m_p = 1.508 * 10^{-4}$ while excitation is located at DG2

In all the investigated case studies, the error in estimating the dominant modes is found to be within 3 percent of the actual modes providing sufficient confidence in assessing the overall microgrid stability regardless of the network X/R ratio, the operating point, or even the excitation location. The process of identifying the dominant modes is simple and can be automatically implemented for small, medium, and large-scale microgrids. Although a communication network is required to collect real-time measurements, the collected data is a small portion of the measurements available at each DG location, so data transmission does not require high bandwidth. Given the available industrial communication protocols within the smart grid concept, the developed stability assessment algorithm should be a viable option and presents a useful tool for online microgrid stability assessment.

V. CONCLUSION

In this paper, an online stability assessment tool for islanded microgrids is proposed based on subspace system identification. The developed algorithm requires introducing a small perturbation in the active droop gain that is quickly restored to its nominal value. The use of subspace identification does not require pre-defining the system's order and avoids the exhaustive computations associated with iterative identification methods. The subspace identification approach showed high accuracy, precision, and reliability in estimating the dominant modes under different operating conditions and network X/R ratio without the need for model reduction techniques or offline analytical models. Furthermore, it has been shown that the proposed online identification method is capable of estimating accurately the dominant modes at various DG locations. The proposed online stability assessment approach is capable of accurately identifying the dominant modes, critical to microgrid stability, and thus can serve as a useful tool in the decision making process for microgrid operators.

REFERENCES

[1] H. Nikkhajoei and R.H. Lasseter, "Distributed generation interface to the CERTS microgrid," *IEEE transactions on power delivery*, vol. 24, no. 3, pp. 1598-1608, 2009.

[2] Olivares, Daniel E.; et al., "Trends in Microgrid Control," *IEEE Transactions on Smart Grid*, vol. 5, no. 4, pp. 1905-1919, July 2014.

[3] Y. Han, H. Li, P. Shen, E. A. A. Coelho and J. M. Guerrero, "Review of Active and Reactive Power Sharing Strategies in Hierarchical

Controlled Microgrids," *IEEE Transactions on Power Electronics*, vol. 32, no. 3, pp. 2427-2451, March 2017.

[4] M.C. Chandorkar, D.M. Divan and R. Adapa, "Control of parallel connected inverters in standalone AC supply systems," *IEEE Transactions on Industry Applications*, vol. 29, no. 1, pp. 136-143, 1993.

[5] J.P. Lopes, C.L. Moreira and A.G. Madureira, "Defining control strategies for microgrids islanded operation," *IEEE Transactions on power systems*, vol. 21, no. 2, pp. 916-924, May 2006.

[6] M. Savaghebi, A. Jalilian, J.C. Vasquez and et al, "Secondary control scheme for voltage unbalance compensation in an islanded droop-controlled," *IEEE Trans. Smart Grid*, vol. 3, no. 2, p. 797–807, June 2012.

[7] E. S. N. Raju P. and T. Jain, "A Two-Level Hierarchical Controller to Enhance Stability and Dynamic Performance of Islanded Inverter-Based Microgrids With Static and Dynamic Loads," *IEEE Transactions on Industrial Informatics*, vol. 15, no. 5, pp. 2786-2797, May 2019.

[8] Q. Zhou, Z. Li, Q. Wu and M. Shahidehpour, "Two-Stage Load Shedding for Secondary Control in Hierarchical Operation of Islanded Microgrids," *IEEE Transactions on Smart Grid*, vol. 10, no. 3, pp. 3103-3111, May 2019.

[9] T. Qian, Y. Liu, W. Zhang, W. Tang and M. Shahidehpour, "Event-Triggered Updating Method in Centralized and Distributed Secondary Controls for Islanded Microgrid Restoration," *IEEE Transactions on Smart Grid,*, vol. 11, no. 2, pp. 1387-1395, March 2020.

[10] Y. Wang, P. Liu, D. Liu, F. Deng and Z. Chen, "Enhanced Hierarchical Control Framework of Microgrids with Efficiency Improvement and Thermal Management," *IEEE Transactions on Energy Conversion*, Early Access.

[11] J. M. Guerrero, J. C. Vasquez, J. Matas, L. G. d. Vicuna and M. Castilla, "Hierarchical Control of Droop-Controlled AC and DC Microgrids—A General Approach Toward Standardization," *IEEE Transactions on Industrial Electronics*, vol. 58, no. 1, pp. 158-172, Jan. 2011.

[12] A. Bidram and A. Davoudi, "Hierarchical Structure of Microgrids Control System," *IEEE Transactions on Smart Grid*, vol. 3, no. 4, pp. 1963-1976, Dec. 2012.

[13] D. I. Brandao, W. M. Ferreira, A. M. S. Alonso, E. Tedeschi and F. P. Marafão, "Optimal Multiobjective Control of Low-Voltage AC Microgrids: Power Flow Regulation and Compensation of Reactive Power and Unbalance," *IEEE Transactions on Smart Grid*, vol. 11, no. 2, pp. 1239-1252, March 2020.

[14] A. Vasilakis, I. Zafeiratou, D. T. Lagos and N. D. Hatziargyriou, "The Evolution of Research in Microgrids Control," *IEEE Open Access Journal of Power and Energy*, vol. 7, pp. 331-343, 2020.

[15] J. M. Guerrero, M. Chandorkar, T. Lee and P. C. Loh, "Advanced Control Architectures for Intelligent Microgrids—Part I: Decentralized and Hierarchical Control," *IEEE Transactions on Industrial Electronics*, vol. 60, no. 4, pp. 1254-1262, April 2013.

[16] K. Ahmed, M. Seyedmahmoudian, S. Mekhilef., N. Mubarak and A. Stojcevski, "A Review on Primary and Secondary Controls of Inverter-Interfaced Microgrid," *Journal of Modern Power Systems and Clean Energy*, Early Access.

[17] N. Pogaku, M. Prodanovic and T.C. Green, "Modeling, analysis and testing of autonomous operation of an inverter-based microgrid," *IEEE Transactions on power electronics*, vol. 22, no. 2, pp. 613-625, Mar. 2007.

[18] A. Kahrobaeian and Y.A.R.I. Mohamed, "Analysis and mitigation of low frequency instabilities in autonomous medium-voltage converter-based microgrids with dynamic loads," *IEEE Trans. Ind. Electron.*, vol. 61, no. 4, p. 1643–1658, 2014.

[19] X. Tang, W. Deng and Z. Qi, "Investigation of the Dynamic Stability of Microgrid," *IEEE Transactions on Power Systems*, vol. 29, no. 2, pp. 698-706, March 2014.

[20] G. Raman and J. C. Peng, "Mitigating Stability Issues Due to Line Dynamics in Droop-Controlled Multi-Inverter Systems," *IEEE Transactions on Power Systems*, vol. 35, no. 3, pp. 2082-2092, May 2020.

[21] N. Bottrell, M. Prodanovic and T.C. Green, "Dynamic stability of a microgrid with an active load," *IEEE Trans. Power Electron.*, vol. 28, no. 11, p. 5107–5119, 2013.

[22] A. A. N. Lasheen, M. Ammar, H. H. Zeineldin, A. Al-Durra, M. F. Shaaban and E. F. El-Saadany, "Assessing the Impact of Reactive Power Droop on Inverter Based Microgrid Stability," *IEEE Transactions on Energy Conversion*, Early Access.

[23] S. P. Nandanoori, S. Kundu, W. Du, F. K. Tuffner and K. P. Schneider, "Distributed Small-Signal Stability Conditions for Inverter-Based Unbalanced Microgrids," *IEEE Transactions On Power Systems*, vol. 35, no. 5, pp. 3981-3990, Sept. 2020.

[24] Y.A.R.I. Mohamed and E.F. El-Saadany, "Adaptive decentralized droop controller to preserve power sharing stability of paralleled inverters in distributed generation microgrids," *IEEE Transactions on Power Electronics*, vol. 23, no. 6, pp. 2806-2816, Dec. 2008.

[25] M.B. Delghavi and A. Yazdani, "An adaptive feedforward compensation for stability enhancement in droop-controlled inverter-based microgrids," *IEEE Transactions on Power Delivery*, vol. 26, no. 3, pp. 1764-1773, Apr. 2011.

[26] H. Mahmood, D. Michaelson and J. Jiang, "Reactive power sharing in islanded microgrids using adaptive voltage droop control," *IEEE Transactions on Smart Grid*, vol. 6, no. 6, pp. 3052-3060, Apr. 2015.

[27] Z. Li, K. W. Chan, J. Hu and J. M. Guerrero, "Adaptive Droop Control Using Adaptive Virtual Impedance for Microgrids with Variable PV Outputs and Load Demands," *IEEE Transactions on Industrial Electronics*, Early Access.

[28] L. Ma and J. Zhang, "An Adaptive Hierarchical Control Method for Microgrid Considering Generation Cost," *IEEE Access*, vol. 8, pp. 164187-164199, 2020.

[29] B. Alghamdi and C. A. Cañizares, "Frequency Regulation in Isolated Microgrids Through Optimal Droop Gain and Voltage Control," *IEEE Transactions on Smart Grid*, Early Access.

[30] S. d. J. M. Machado, S. A. O. d. Silva, J. R. B. d. A. Monteiro and A. A. d. Oliveira, "Network Modeling Influence on Small-Signal Reduced-Order Models of Inverter-Based AC Microgrids Considering Virtual Impedance," *IEEE Transactions on Smart Grid*, vol. 12, no. 1, pp. 79-92, Jan. 2021.

[31] P. V. Overschee and B. D. Moor, Subspace Identification For Linear Systems Theory - Implementation - Applications, Belgium: Kluwer Academic, 1996.